Chapter 1

A Further Look at Q_1 and Q_2 from TOGA COARE

RICHARD H. JOHNSON AND PAUL E. CIESIELSKI

Colorado State University, Fort Collins, Colorado

THOMAS M. RICKENBACH

Department of Geography, Planning, and Environment, East Carolina University, Greenville, North Carolina

ABSTRACT

Two features of Yanai et al.'s profiles of Q_1 and Q_2—the commonly observed double-peak structure to Q_2 and an inflection in the Q_1 profile below the melting level—are explored using estimates of convective and stratiform rainfall partitioning based on Massachusetts Institute of Technology (MIT) radar reflectivity data collected during TOGA COARE. The MIT radar data allow the Q_1 and Q_2 profiles to be classified according to stratiform rain fraction within the radar domain and, within the limitations of the datasets, allow interpretations to be made about the relative contributions of convective and stratiform precipitation to the mean profiles. The sorting of Q_2 by stratiform rain fraction leads to the confirmation of previous findings that the double-peak structure in the mean profile is a result of a combination of separate contributions of convective and stratiform precipitation. The convective contribution, which has a drying peak in the lower troposphere, combines with a stratiform drying peak aloft and low-level moistening peak to yield a double-peak structure. With respect to the inflection in the Q_1 profile below the 0°C level, this feature appears to be a manifestation of melting. It is the significant horizontal dimension of the stratiform components of tropical convective systems that yields a small but measurable imprint on the large-scale temperature and moisture stratification upon which the computations of Q_1 and Q_2 are based. The authors conclude, then, that the rather subtle features in the Q_1/Q_2 profiles of Yanai et al. are directly linked to the prominence of stratiform precipitation within tropical precipitation systems.

1. Introduction

A conceptual breakthrough in understanding how tropical cloud systems interact with their environment was achieved through the landmark paper of Yanai et al. (1973), wherein the now-familiar Q_1 (apparent heat source) and Q_2 (apparent moisture sink) were defined. However, well prior to the 1973 study, Yanai (1961) introduced Q_1 and Q_2 in a paper titled "A detailed analysis of typhoon formation," which investigated the dynamic and thermodynamic properties of the formation of Typhoon Doris (1958) in the western Pacific. Vertical profiles of Q_1 and Q_2—the first ever to be presented—were shown in Yanai (1961) for the period of the transformation of Doris from a cold-core to warm-core tropical cyclone.

Following Yanai et al. (1973), but including ice processes, we write the equations for the apparent heat source and moisture sink as follows:

$$Q_1 \equiv \frac{\partial \overline{s}}{\partial t} + \overline{\mathbf{v}} \cdot \nabla \overline{s} + \overline{\omega} \frac{\partial \overline{s}}{\partial p}$$
$$= L_v(\overline{c} - \overline{e}) + (L_v + L_f)(\overline{d} - \overline{s}_*)$$
$$+ L_f(\overline{f} - \overline{m}) + Q_R - \frac{\partial}{\partial p}(\overline{s'\omega'}), \quad \text{and} \quad (1\text{-}1)$$

$$Q_2 \equiv -L_v\left(\frac{\partial \overline{q}}{\partial t} + \overline{\mathbf{v}} \cdot \nabla \overline{q} + \overline{\omega} \frac{\partial \overline{q}}{\partial p}\right)$$
$$= L_v(\overline{c} - \overline{e}) + L_v(\overline{d} - \overline{s}_*) + L_v \frac{\partial}{\partial p}(\overline{q'\omega'}), \quad (1\text{-}2)$$

where c, e, d, s_*, f, and m are condensation, evaporation, deposition, sublimation, freezing, and melting rates,

Corresponding author address: Richard H. Johnson, Department of Atmospheric Science, Colorado State University, 3915 W. Laport Ave., Fort Collins, CO 80523.
E-mail: johnson@atmos.colostate.edu

DOI: 10.1175/AMSMONOGRAPHS-D-15-0002.1

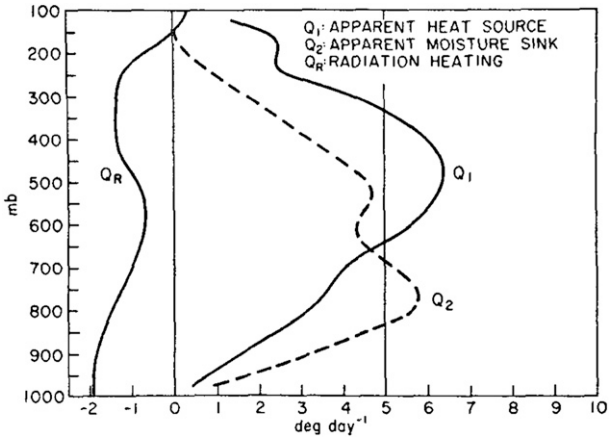

FIG. 1-1. Apparent heat source Q_1, apparent moisture sink Q_2, and net radiative heating rate Q_R for the Marshall Islands. From Yanai et al. (1973).

respectively; q is the water vapor mixing ratio; $s \equiv c_p T + gz$ is the dry static energy; Q_1 is the apparent heat source; Q_2 is the apparent moisture sink; Q_R is the net radiative heating rate; L_v and L_f are the latent heats of vaporization and fusion, respectively; the overbar refers to a horizontal average; and the primes denote a deviation from this average.

Yanai et al. (1973) used 1956 Marshall Islands sounding data to compute Q_1 and Q_2 and then applied a simplified cloud model to diagnose the bulk properties of cumulus ensembles, which provided substantial insight into the properties of tropical convective systems and how they impact their environment. The profiles of Q_1 and Q_2 obtained by Yanai et al. (1973) for the Marshall Islands for the period 15 April–22 July 1956 are shown in Fig. 1-1, along with radiative heating Q_R estimates from Dopplick (1972, 1979). They found a primary peak in Q_1 in the upper troposphere, whereas the principal Q_2 peak was in the lower troposphere. Yanai et al. (1973) pointed out that the separation of the Q_1 and Q_2 peaks is indicative of vigorous deep convection [i.e., strong vertical eddy fluxes of moist static energy $h(\equiv s + L_v q)$]. Since the profiles are averages over a 3-month period, they represent contributions from both convective and stratiform components of precipitation systems, which have distinctly different heating and moistening profiles (Houze 1982, 1989; Johnson 1984). Just how the structure of the heating profile varies in the vertical is of considerable interest, since that determines the dynamical response of the environment to convection (Hartmann et al. 1984; Raymond and Jiang 1990; Nicholls et al. 1991; Schumacher et al. 2004).

A curious feature of the Q_2 profile is its double-peaked structure, which has also been found for the GARP Atlantic Tropical Experiment (GATE)

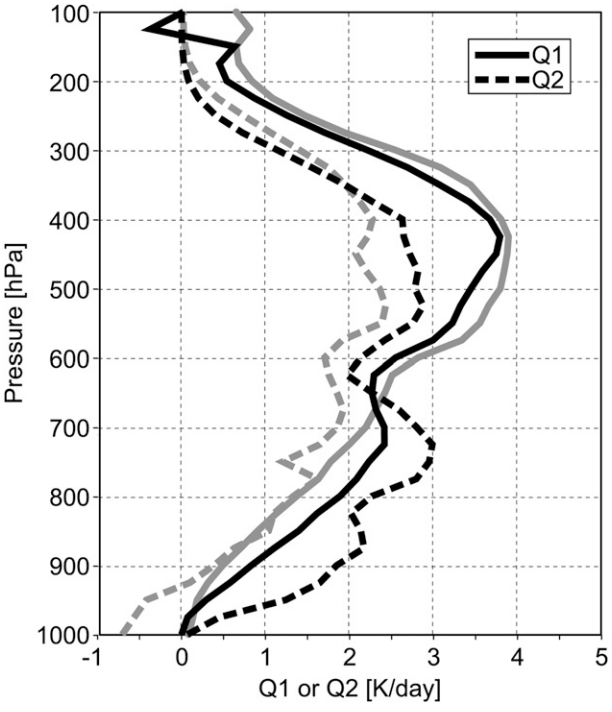

FIG. 1-2. Apparent heat source Q_1 and apparent moisture sink Q_2 for MISMO in the Indian Ocean (dark curve) and TOGA COARE Intensive Flux Array (light curve). From Katsumata et al. (2011).

(Esbensen et al. 1988), as well as for other experiments such as the more recent R/V *Mirai* Indian Ocean Cruise for the Study of the Madden–Julian oscillation (MJO) Onset (MISMO) (Katsumata et al. 2011). This feature has been attributed by Johnson (1984) and Esbensen et al. (1988) to the separate contributions of

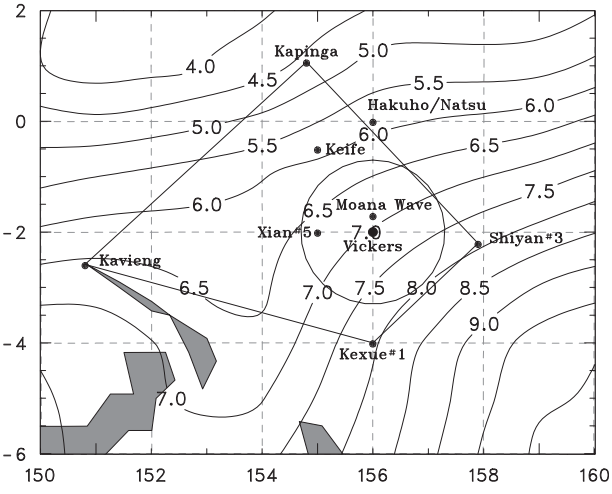

FIG. 1-3. TOGA COARE Intensive Flux Array quadrilateral, atmospheric sounding sites, and 4-month mean TOGA COARE rainfall (mm day^{-1}) from the Global Precipitation Climatology Project (GCPC). The circle indicates the 120-km radius radar study area. MIT radar was on board R/V *Vickers*.

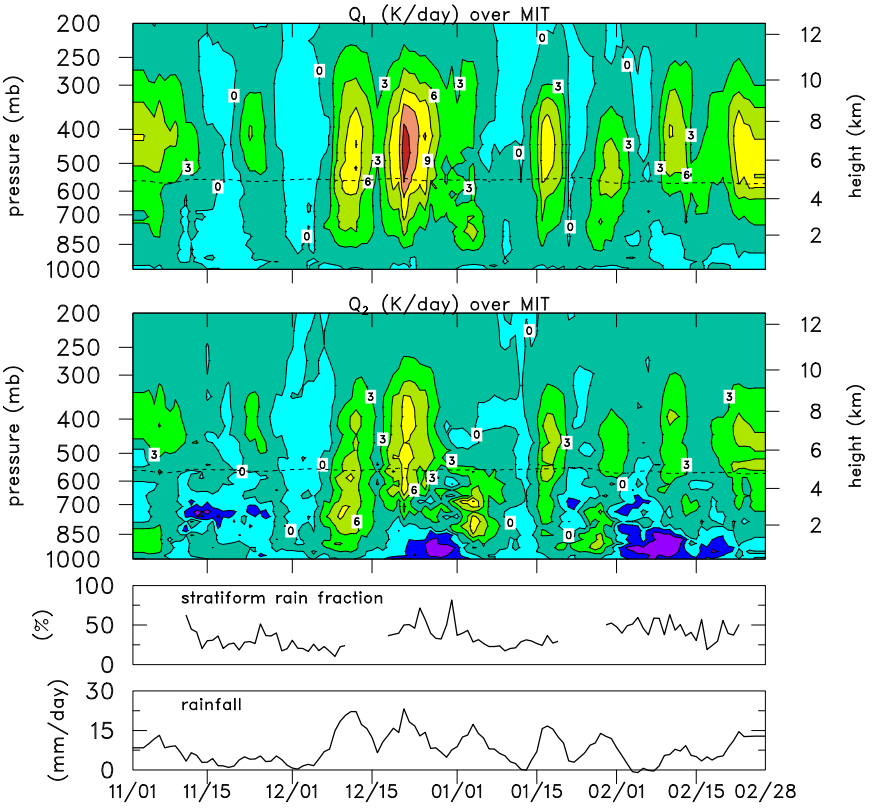

FIG. 1-4. (top to bottom) TOGA COARE IOP time series of Q_1 and Q_2 (dashed line indicates the 0° level), time series of stratiform rain fraction, and moisture-budget-derived rainfall. Budget fields and rainfall have been smoothed with a 5-day running mean filter. All fields are for MIT radar area.

convective and stratiform precipitation systems. Namely, condensation and deposition aloft associated with stratiform precipitation produces the upper peak while condensation in convective precipitation produces the lower peak. Placed in a time perspective, the vertical motion and hence heating and drying typically undergo an evolution (on time scales ranging from diurnal to the life cycle of tropical cloud clusters to the passage of easterly waves) from a low-level peak in the vertical motion (and heating) in the early stages to an upper-level peak in the later stages (Frank 1978; Nitta 1978; Houze 1982; Johnson and Young 1983). This evolution has since been documented on longer time scales ranging up to the 30–60-day MJO, as reviewed by Kiladis et al. (2009).

It is the purpose of this article to delve further into the relationship between the Q_1 and Q_2 profiles and convective/stratiform rain partitioning using radar and sounding data from an experiment, which is now celebrating its twenty-third anniversary—the 1992–93 Tropical Ocean and Global Atmosphere Coupled Ocean–Atmosphere Response Experiment (TOGA COARE)—conducted in the western Pacific (Webster and Lukas 1992). However, we first note that the experiment-mean TOGA COARE Q_1 and Q_2 profiles (Johnson and Ciesielski 2000) are different from those of the Marshall Islands, GATE, and MISMO. To illustrate this difference, a comparison of the mean profiles for MISMO and TOGA COARE is shown in Fig. 1-2 (from Katsumata et al. 2011). Notably absent from the TOGA COARE results are low-level peaks in heating and drying. This behavior was also found over the northern South China Sea during the May–June 1998 South China Sea Monsoon Experiment (SCSMEX; Johnson and Ciesielski 2002). Johnson and Lin (1997) explained the unique feature of the TOGA COARE profiles as a consequence of frequent trade wind–like, nonprecipitating cumulus clouds during the quiescent and westerly wind burst phases of the MJO. These clouds were prevalent during dry midtropospheric conditions and served to moisten the lower troposphere, thereby producing prolonged periods of negative Q_2, as also observed during the Barbados Oceanographic and Meteorological Experiment (BOMEX; Nitta and Esbensen 1974). In contrast, during the active phase of the MJO, Q_1 and Q_2 distributions much like those of Yanai et al. (1973) were observed [Fig. 3 of Johnson and Lin (1997)].

In this chapter we will use radar data from the Massachusetts Institute of Technology (MIT) radar on board the R/V *Vickers* during TOGA COARE (Rickenbach and Rutledge 1998) to relate the heating and moistening profiles to the stratiform/convective rain fractions derived by that radar to further elucidate the factors contributing to the observed mean Q_1 and Q_2 profiles for that experiment.

2. Data and analysis procedures

a. Radar data

Radar reflectivity data from the MIT C-band Doppler radar, deployed on board the R/V *Vickers* and processed as described in Rickenbach and Rutledge (1998), are used in this study. The position of the *Vickers* within the TOGA COARE Intensive Flux Array (IFA) is shown in Fig. 1-3 along with other sounding sites in the region used in the budget analyses. Rickenbach and Rutledge (1998, see their Fig. 2) indicate the time periods of the radar and sounding operations during the 4-month TOGA COARE intensive observing period (IOP; November 1992–February 1993). Convective/stratiform rain partitioning was carried out using a slight modification of the method of Steiner et al. (1995) applied to 10-min radar reflectivity volumes. The mean stratiform rain fraction for the three cruises of the *Vickers* was determined to be 28%, which is less than the ~40% estimate for this region by Schumacher and Houze (2003) obtained from the Tropical Rainfall Measuring Mission (TRMM) Precipitation Radar (PR). However, as we will see later, the MIT-based estimate is closer to the TRMM-based value if we remove the periods of trade wind cumulus from the average. We would expect this to be the case since the 4–5-km footprint of the PR tends to smooth out and lower the reflectivity of the precipitating cumulus (the so-called "beamfilling" problem) compared to the higher-resolution MIT shipborne radar.

b. Sounding data and averaging methodology

The 6-hourly sounding data were objectively analyzed onto a 1° × 1° grid at 25-hPa intervals from 1000 to 25 hPa over the large-scale TOGA COARE domain using procedures described in Ciesielski et al. (1997), and incorporating humidity sensor corrections as outlined in Ciesielski et al. (2003). The resulting gridded basic and derived fields were then averaged over the circular MIT radar coverage area shown in Fig. 1-3. The distribution of sounding sites in proximity to the *Vickers* is reasonably good, so analyses over this region are deemed fairly reliable, apart from other issues such as temporal data gaps and random sampling errors (Mapes et al. 2003).

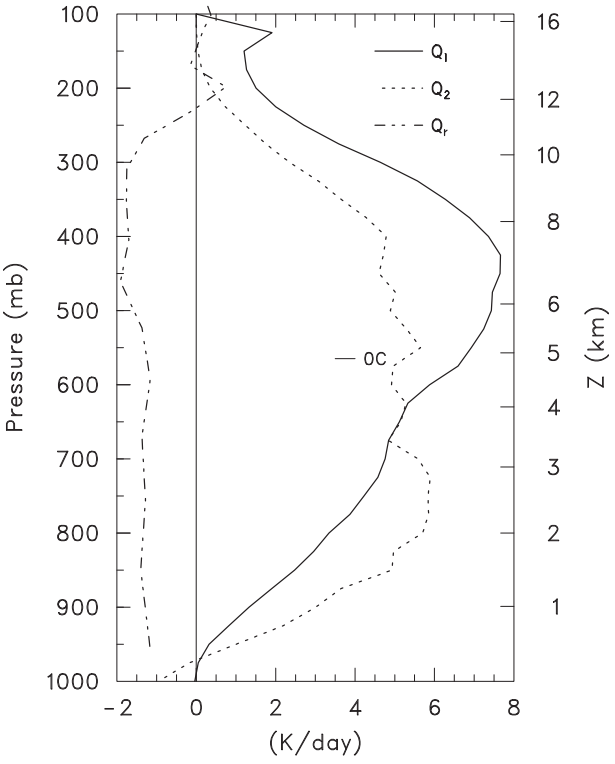

FIG. 1-5. Average Q_1 and Q_2 profiles for MIT radar coverage area for times when precipitation from the atmospheric moisture budget over this area exceeded 3.5 mm day^{-1}. The Q_R profile is from L'Ecuyer and Stephens (2003) based on 13-yr (1998–2011) mean over this region. The 0°C level is indicated.

3. Results for the 4-month TOGA COARE intensive observing period

A time series of Q_1 and Q_2 for the TOGA COARE IOP is shown in Fig. 1-4, along with the stratiform rainfall fraction based on MIT radar data for the three cruises of the *Vickers* and average rainfall for the MIT radar coverage area derived from the moisture budget, where the Woods Hole Oceanographic Institution Improved Meteorology (IMET) buoy is used for surface evaporation. A prominent MJO event occurred in December, characterized by a transition from shallow convection (low-level peak in Q_2) early in the month followed by deep convection midmonth and then stratiform precipitation (drying above moistening) at the end of the month (Lin and Johnson 1996). Consistent with this evolution is an increasing trend in the stratiform rainfall fraction through December as determined by the MIT radar.

Conspicuous in Fig. 1-4 are several ~10-day to 2-week periods of negative Q_2 in the lower troposphere, namely, near 750 hPa in mid-November and near 900 hPa in late December and early February. These features were described by Johnson and Lin (1997) as episodes of trade wind–like shallow cumulus existing during very

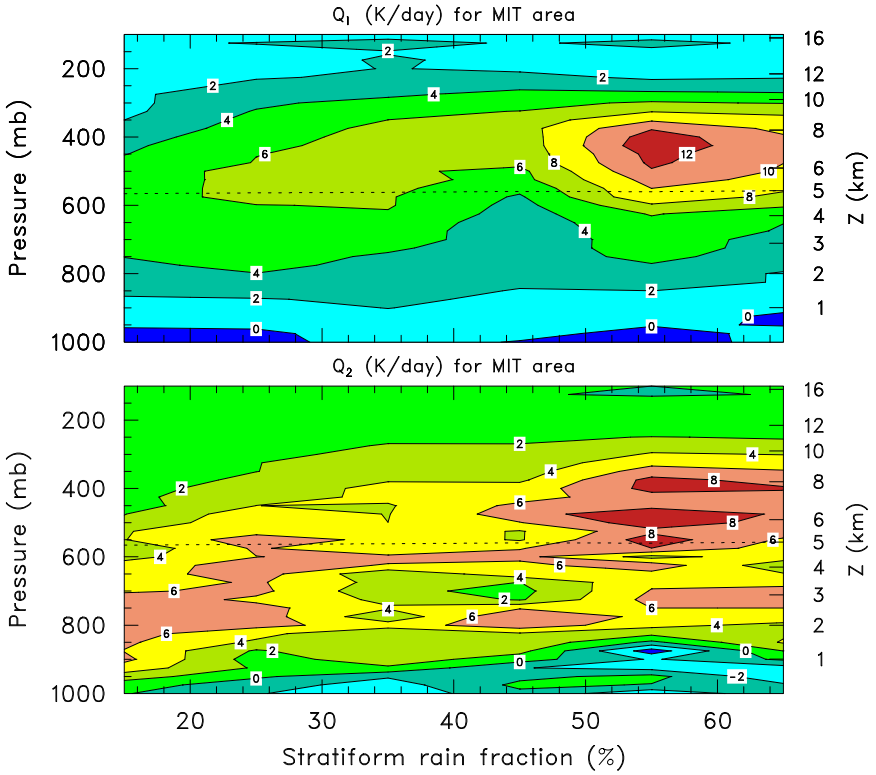

FIG. 1-6. The (top) Q_1 and (bottom) Q_2 (K day^{-1}) as a function of stratiform rain fraction for the MIT radar coverage area during TOGA COARE for times when moisture-budget-derived rainfall over that area exceeded 3.5 mm day^{-1} (dashed line indicates the 0°C level).

dry low- to midtroposphere conditions. The moistening in November occurred during light surface wind conditions, whereas the episodes in late December and February were during strong winds. They noted that when winds were strong during these shallow cumulus periods, there was greater moistening (negative Q_2) near the cloud base in association with subinversion-type (Esbensen 1978) or forced-type (Stull 1985) cumuli that were, in part, a manifestation of overshooting boundary layer eddies. When winds were light, the cumuli were slightly deeper ["inversion penetrating" after Esbensen (1978) or "active" after Stull (1985)] and the moistening peaked in the upper part of the cloud layer [similar to the Atlantic trades; Nitta and Esbensen (1974)]. Higher sea surface temperatures (by 1 K) and weaker shear observed during the November period likely contributed to the more active cumuli at that time.

4. Relating Q_1 and Q_2 to stratiform rain fraction

The frequent occurrence of trade wind regimes over the warm pool during TOGA COARE can be attributed to "dry intrusions" that were observed in association with the MJO (Parsons et al. 1994; Numaguti et al. 1995; Yoneyama and Fujitani 1995; Mapes and Zuidema 1996), which helped to inhibit the growth of convection (e.g., Redelsperger et al. 2002). Johnson and Lin (1997) focused on Q_1 and Q_2 during these trade wind–like periods by averaging the profiles for times when precipitation was less than 3.5 mm day^{-1}, the average surface evaporation rate during TOGA COARE. Alternatively, to explore the characteristics of deep convection during TOGA COARE, we remove the effects of these periods by including only those times when the precipitation exceeded 3.5 mm day^{-1}. The resulting Q_1/Q_2 profiles are shown in Fig. 1-5. They now look much like those of Yanai et al. (1973) (see Fig. 1-1), namely, possessing a double-peak structure to Q_2 (though with several additional peaks) and an inflection in the Q_1 profile near 650 hPa.[1] Therefore, to interpret the Yanai

[1] Both the Marshall Islands and the western Pacific Q_1 profiles also show peaks near 150 hPa. These peaks may not represent any physical processes, rather they may be artifacts of applying the boundary condition $\omega = 0$ at the tropopause or 100 hPa such that some upward motion acting on weak stability above the lapse-rate minimum (Fueglistaler et al. 2009) produces a local heating maximum.

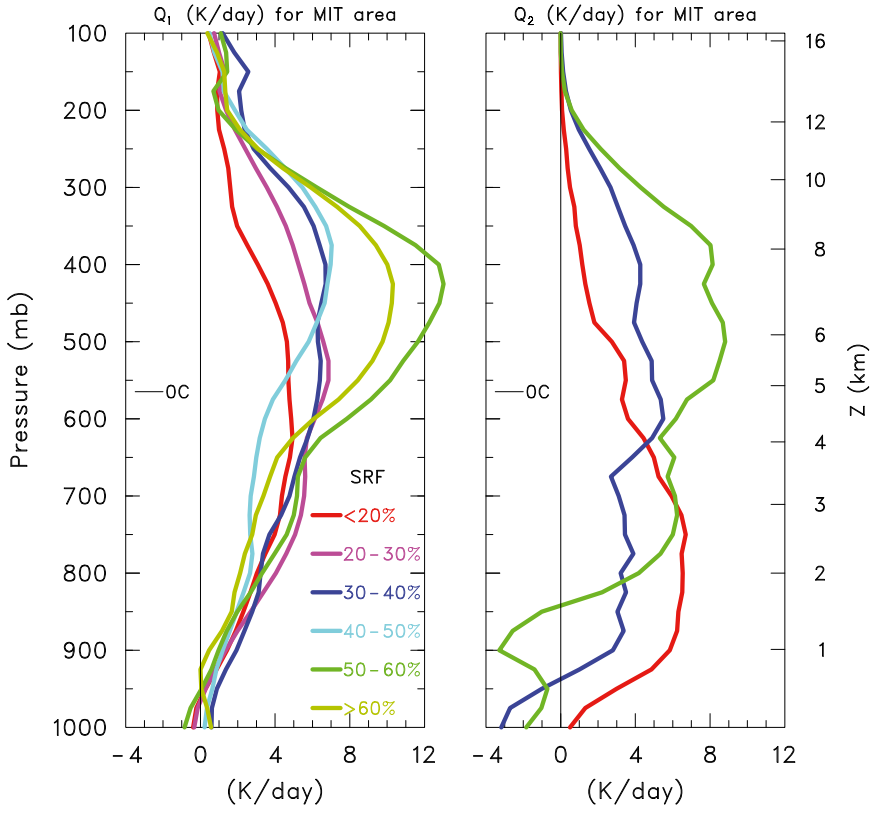

FIG. 1-7. The Q_1 and Q_2 profiles as a function of stratiform rain fraction (SRF) for the MIT radar coverage area during TOGA COARE for times when moisture-budget-derived rainfall over that area exceeded 3.5 mm day^{-1}. SRF values plotted for Q_1 are averages for the following SF bins: <20%, 20%–30%, 30%–40%, 40%–50%, 50%–60%, and >60%. Values for Q_2 are plotted only for <20%, 30%–40%, and 50%–60% for the sake of clarity. Curves have been smoothed in the vertical with a 1–2–1 filter.

et al. (1973) profiles in light of the TOGA COARE results, we subsequently restrict analyses to the dates and times that make up Fig. 1-5 (184 total 6-h periods). In support of this procedure, we note that an inflection in the Q_1 profile was also found by Schumacher et al. (2007) for the heavy-rain threshold cases of SCSMEX and the 1999 Kwajalein Experiment (KWAJEX).

The Q_1 and Q_2 profiles as a function of stratiform rain fraction (SRF) are shown in Fig. 1-6. As SRF increases, there is a transition from vertically separated, single peaks in heating and drying in the low- to midtroposphere to nearly coincident peaks at higher levels, consistent with an evolution in the precipitation from mostly convective to mainly stratiform in character (Luo and Yanai 1984). The evolution for Q_2 is more complex than that for Q_1, with multiple drying peaks aloft above a moistening peak in the lower troposphere. The low-level drying peaks between 700 and 800 hPa for SRF > 40% likely reflect the effects of convection coexisting with stratiform precipitation (Leary and Houze 1979).

Another way of viewing this transition is by comparing profiles for different values of SRF (Fig. 1-7). In this plot SRF values shown are averages for the following SRF bins: <20%, 20%–30%, 30%–40%, 40%–50%, 50%–60%, and >60%. The number of cases in each bin is 41, 53, 29, 17, 15, and 29, respectively. Although there is noise in the profiles (especially for Q_2, where results for only three bins are shown), the transition from convective to stratiform structure with increasing SRF can clearly be seen. Also evident for large values of SRF is an inflection in the Q_1 profile below 0°C near 4 km. This feature has been attributed to cooling by melting, which has been seen in observations (e.g., Johnson et al. 1996) and cloud-resolving models (e.g., Shie et al. 2003). The inflection in Q_1 is also observed in the Yanai et al. (1973) Marshall Islands Q_1 profile (Fig. 1-1).

Because of the abundant precipitation over the warm pool, melting leaves a measurable and persistent effect on the static stability. Melting takes place over a relatively shallow layer [~300–400 m deep; Willis and Heymsfield (1989)] below the 0°C level. Freezing of

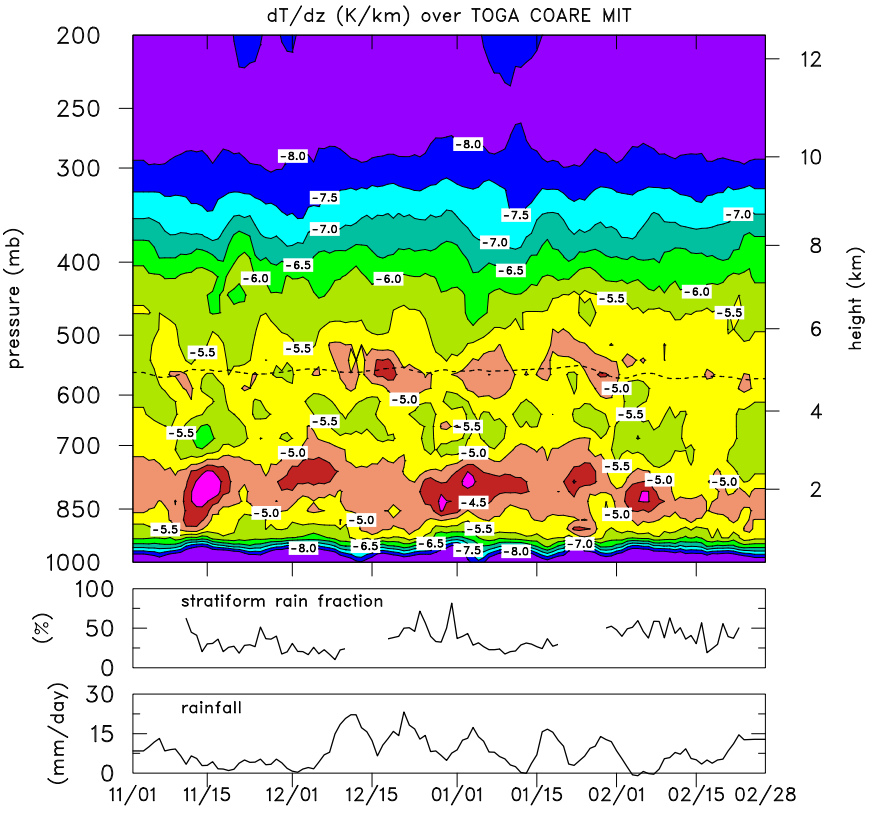

FIG. 1-8. (top) TOGA COARE intensive observing period time series of static stability dT/dz (K km^{-1}) (dashed line indicates the 0° level), (middle) time series of stratiform rain fraction, and (bottom) moisture-budget-derived rainfall. All fields are for MIT radar area.

hydrometeors occurs at levels above 0°C, but over a deeper layer; nevertheless, the combined effects of freezing above melting serves to increase the static stability at the 0°C level and also from $L_v(\overline{f} - \overline{m})$ in (1-1), the vertical gradient in Q_1 there. However, when computing Q_1 from sounding data, it is the lhs of (1-1) that is calculated and, since the vertical advection term $\overline{\omega}\partial\overline{s}/\partial p$ is usually the dominant term in that calculation, the impact of freezing and melting perturbs $\partial\overline{s}/\partial p$ and hence the Q_1 profile. To illustrate this effect, a time series of static stability, represented as dT/dz in Fig. 1-8, shows a persistent stable layer in proximity to 0°C. This stable layer is strongest during periods of heaviest rainfall, so its linkage to melting is perceptible. Also seen in Fig. 1-8

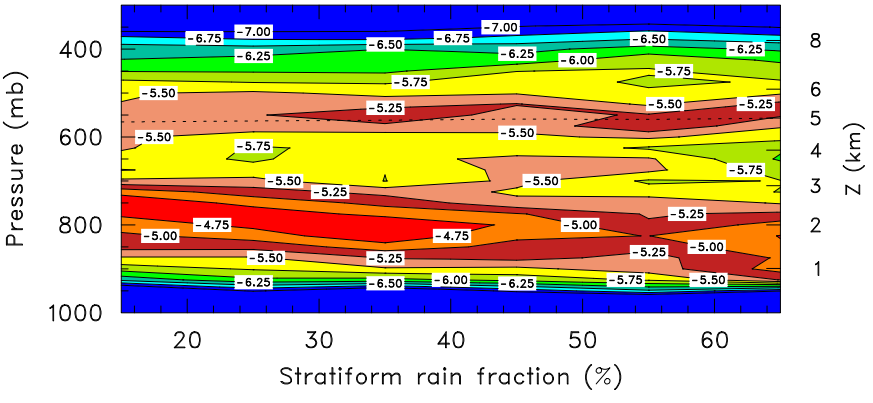

FIG. 1-9. Static stability dT/dz (K km^{-1}) as a function of stratiform rain fraction for the MIT radar coverage area during TOGA COARE for times when moisture-budget-derived rainfall over that area exceeded 3.5 mm day^{-1}.

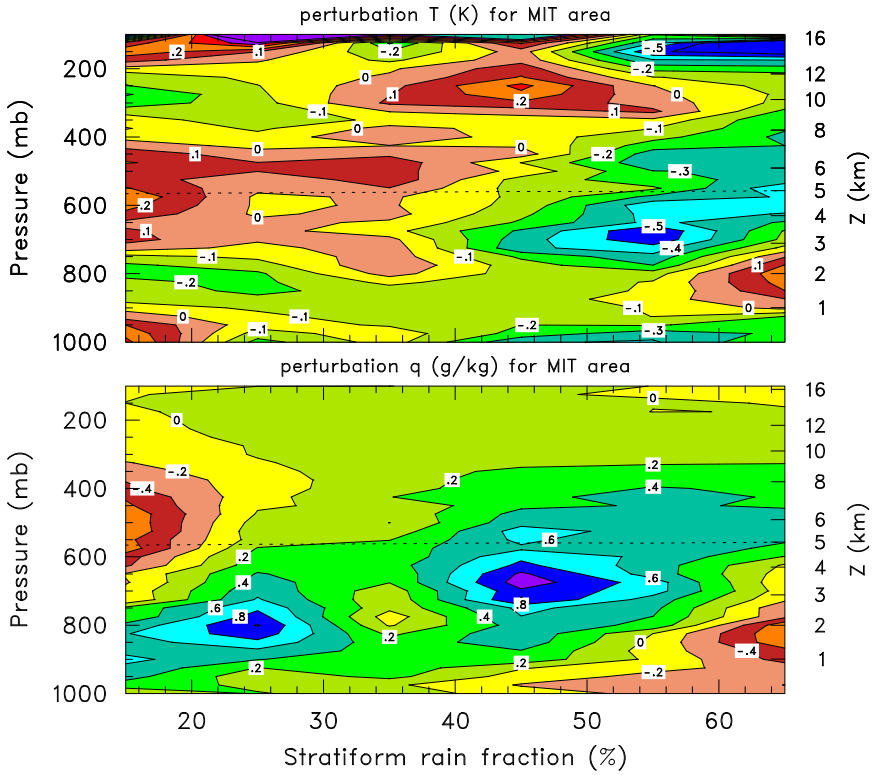

FIG. 1-10. (top) Perturbation temperature (K; deviation from IOP mean) and (bottom) perturbation water vapor mixing ratio (g kg^{-1}) as a function of stratiform rain fraction for the MIT radar coverage area during TOGA COARE for times when moisture-budget-derived rainfall over that area exceeded 3.5 mm day^{-1} (dashed line indicates the 0°C level).

is a persistent, though fluctuating in intensity, trade wind stable layer, which tends to be strongest during periods of light rainfall and negative low-level Q_2 (Fig. 1-4).

To further elucidate the relationship between the melting stable layer and stratiform precipitation, dT/dz is plotted as a function of SRF in Fig. 1-9. As the SRF increases, the strength of the melting stable layer increases, as one would expect considering the associated larger horizontal areas covered by precipitation when the SRF is high. On the other hand, the trade wind stable layer weakens as SRF increases, consistent with the idea that this layer occurs episodically over the warm pool (Johnson and Lin 1997) and is present primarily outside the active phase of the MJO when the SRF is low. In addition, there is a noticeable descent of the height of the trade stable layer as SRF increases. This behavior may be related to the finding of Johnson and Lin (1997) that during light-rain (and light wind) periods of the MJO with small SRF, there is a greater proportion of active trade cumulus (Esbensen 1978; Stull 1985), which rise to higher elevations than during the westerly wind burst phase with high SRF, when "forced" cumuli that are extensions of boundary layer turbulence predominate.

Because the stratiform precipitation systems cover large areas, their impact on the temperature field is significant. This effect is seen in Fig. 1-10, where for SRF $>$ 50%, a shallow cool anomaly is present in a layer below the melting level, accompanied by a deeper moist layer aloft. For the largest values of SRF, there are both warm and dry anomalies centered just below 800 hPa. These features are manifestations of "onion soundings," often observed in association with the stratiform precipitation regions of tropical squall lines or cloud clusters (Zipser 1977). This structure can also be seen in Fig. 1-11, a plot of the mean relative humidity for SRF $>$ 60% and $<$ 20%. For large values of SRF, moist conditions exist above 0°C, indicative of stratiform anvil clouds aloft, with dry conditions below. In contrast, the mostly convective situations (SRF $<$ 20%) are characterized by a relatively dry mid- to upper troposphere but slightly moister conditions below 3 km. The two contrasting profiles in Fig. 1-11 are consistent with the bimodal relative humidity behavior for TOGA COARE reported by Brown and Zhang (1997). For the lowest values of SRF (Fig. 1-10), dry conditions are observed in the midtroposphere, which act to suppress cloud development.

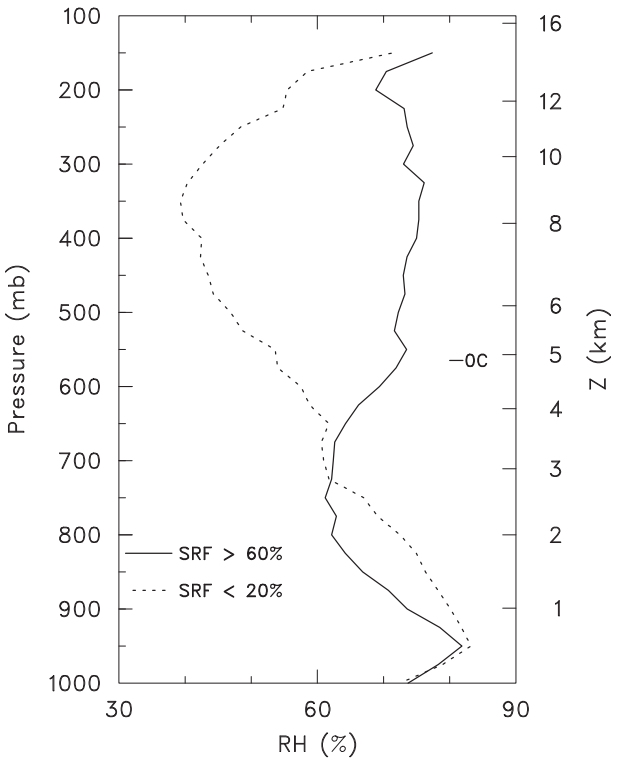

FIG. 1-11. Relative humidity (with respect to ice for $T < 0°C$) for stratiform rain fraction >60% (solid curve) and <20% (dashed curve).

Also observed for large SRF values (Fig. 1-10) is a layer of cooling near the tropopause (~150 hPa), a feature commonly observed atop mesoscale convective systems in the tropics (Johnson and Kreite 1982; Holloway and Neelin 2007). In addition, a cool anomaly is observed near the surface for increasing values of SRF, indicative of extensive modification of the boundary layer by downdrafts as the stratiform rain amounts and associated area coverage increases (Zipser 1977; Fitzjarrald and Garstang 1981).

In the computation of Q_2 from large-scale fields, the dominant term is $\overline{\omega}\partial\overline{q}/\partial p$. The individual contributions to this term are plotted as a function of SRF in Fig. 1-12. There is a clear upward shift in the vertical motion peak (Fig. 1-12, top) as SRF increases. The average SRF for the cases considered here (those for rainfall exceeding 3.5 mm day^{-1}) is 36%, somewhat higher than the 28% for the entire MIT radar period. Viewing the $\overline{\omega}$ variation and noting that half the rain is above SRF = 36% and half below, it is readily apparent that the double-peak structure to Q_2 arises from the individual convective and stratiform contributions. The time series of dq/dp (Fig. 1-12, middle) shows a trend toward a local maximum near the melting layer as SRF increases, reflecting the increasing presence of stratiform clouds with bases near that level (Johnson et al. 1996). To confirm that the term involving $\overline{\omega}\partial\overline{q}/\partial p$ is the principal contributor to Q_2, the SRF-sorted behavior of this term is shown in Fig. 1-12 (bottom). Overall, the broad pattern and evolution of this term is similar to that of Q_2 (Fig. 1-6, bottom), showing distinctly different vertical structures for small and large values of SRF. The greater vertical structure in Q_2 is likely a result of horizontal advection of dry air in thin layers, often occurring near the melting level, which Mapes and Zuidema (1996) and Johnson et al. (1996) found to be prevalent over the western Pacific warm pool during TOGA COARE.

5. Summary and conclusions

It has been over four decades since the landmark paper of Yanai et al. (1973) diagnosing apparent heat sources Q_1 and moisture sinks Q_2, as well as convective transports based on a simplified cloud model, using Marshall Islands data. In subsequent years, numerous field campaigns in the tropics and midlatitudes have been conducted computing Q_1 and Q_2, with results similar to those of Yanai et al. In this chapter we explore aspects of those heating and moistening profiles using estimates of convective and stratiform rainfall partitioning based on MIT radar reflectivity data from the R/V *Vickers* during TOGA COARE (Rickenbach and Rutledge 1998). Particular attention is given to (i) the commonly observed double-peak structure to Q_2 and (ii) an inflection in the Q_1 profile below the melting level, and the relationship of these features to the convective cloud populations.

The MIT radar data allow the Q_1 and Q_2 profiles to be classified according to stratiform rain fraction and, within the limitations of the datasets, interpretations to be made about the relative contributions of convective and stratiform precipitation to the mean profiles. Radar data from the three cruises of the *Vickers* are used along with gridded fields constructed from the TOGA COARE sounding array and averaged over the MIT radar coverage area. To remove periods when trade wind–like cumulus were present during TOGA COARE, times were selected for analysis when the average rainfall rate over the MIT area exceeded 3.5 mm day^{-1}. This criterion resulted in 184 total 6-hourly periods, for which the average stratiform rain fraction was 36%.

The sorting of Q_2 by stratiform rain fraction leads to the conclusion that its double-peak structure is a result of the separate contributions of convective and stratiform precipitation, as suggested by Johnson (1984), Esbensen et al. (1988), and others. The convective contribution gives a lower drying peak, which when combined with the stratiform contribution of a drying peak aloft (along with moistening at low levels), yields the double-peak structure. With respect to the inflection

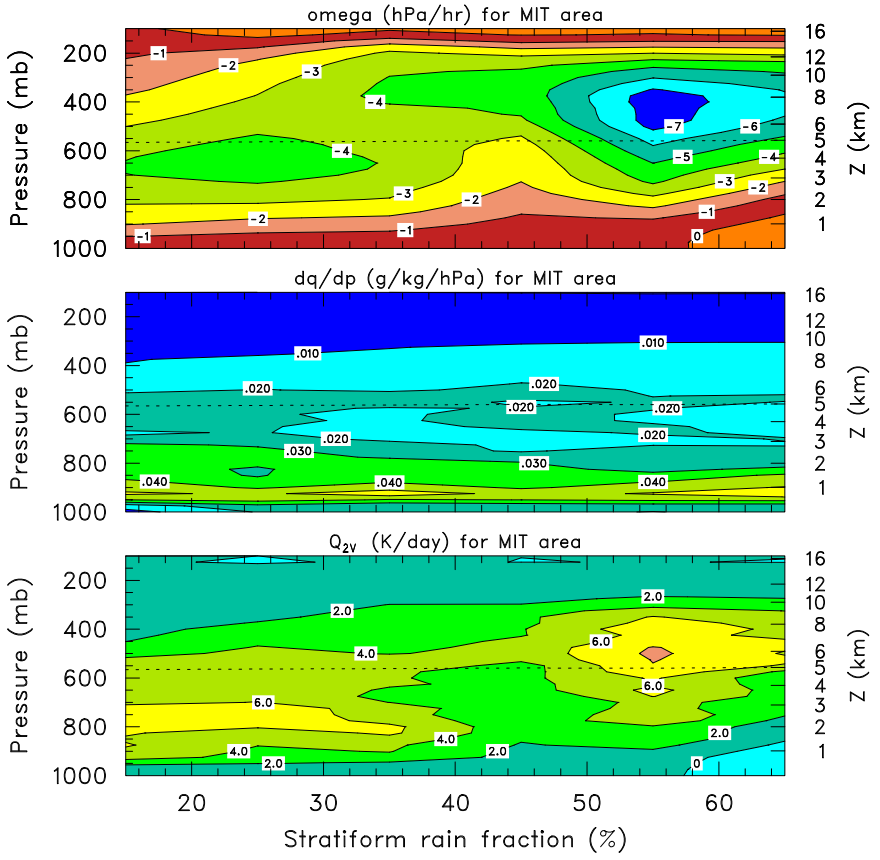

FIG. 1-12. (top) $\overline{\omega}$ (hPa h^{-1}), (middle) $d\overline{q}/dp$ (g kg^{-1} hPa^{-1}), and (bottom) $-L_v\overline{\omega}\partial\overline{q}/\partial p$ (K day^{-1}) as a function of stratiform rain fraction for the MIT radar coverage area during TOGA COARE for times when moisture-budget-derived rainfall over that area exceeded 3.5 mm day^{-1} (dashed line indicates the 0°C level).

in the Q_1 profile below 600 hPa or 4 km, this feature appears to be a manifestation of cooling by melting just below the 0°C level, which has a prominent impact due to the broad areal coverage of stratiform precipitation.

We conclude, then, that the rather subtle features in the Q_1/Q_2 profiles of Yanai et al. (1973) are directly linked to effects of stratiform precipitation systems, years ago identified by Zipser (1969, 1977) and Houze (1977) as integral components of tropical convection. These systems cover large areas and leave behind perturbations to the temperature and moisture stratification in the tropics, which are readily detectable using sounding data. With the recent completion of the Dynamics of the Madden–Julian Oscillation (DYNAMO) field campaign in the Indian Ocean (October 2011–March 2012), the opportunity exists to further extend this analysis to another tropical ocean basin.

Acknowledgments. This article is prepared as a tribute to Michio Yanai in honor of his enormous contributions to the field of atmospheric science. We thank Courtney Schumacher and two anonymous reviewers for their helpful comments on the manuscript. The research has been supported by the National Science Foundation under Grants AGS-0966758, AGS-1059899, and AGS-1118141, and the National Aeronautics and Space Administration under Grant NNX10AG81G.

REFERENCES

Brown, R. G., and C. Zhang, 1997: Variability of midtropospheric moisture and its effect on cloud-top height distribution during TOGA COARE. *J. Atmos. Sci.*, **54**, 2760–2774, doi:10.1175/1520-0469(1997)054<2760:VOMMAI>2.0.CO;2.

Ciesielski, P. E., L. Hartten, and R. H. Johnson, 1997: Impacts of merging profiler and rawinsonde winds on TOGA COARE analyses. *J. Atmos. Oceanic Technol.*, **14**, 1264–1279, doi:10.1175/1520-0426(1997)014<1264:IOMPAR>2.0.CO;2.

——, R. H. Johnson, P. T. Haertel, and J. Wang, 2003: Corrected TOGA COARE sounding humidity data: Impact on diagnosed properties of convection and climate over the warm pool. *J. Climate*, **16**, 2370–2384, doi:10.1175/2790.1.

Dopplick, T. G., 1972: Radiative heating of the global atmosphere. *J. Atmos. Sci.*, **29**, 1278–1294, doi:10.1175/1520-0469(1972)029<1278:RHOTGA>2.0.CO;2.

——, 1979: Radiative heating of the global atmosphere: Corrigendum. *J. Atmos. Sci.*, **36**, 1812–1817, doi:10.1175/1520-0469(1979)036<1812:RHOTGA>2.0.CO;2.

Esbensen, S., 1978: Bulk thermodynamic effects and properties of small tropical cumuli. *J. Atmos. Sci.*, **35**, 826–837, doi:10.1175/1520-0469(1978)035<0826:BTEAPO>2.0.CO;2.

——, J.-T. Wang, and E. I. Tollerud, 1988: A composite life cycle of nonsquall mesoscale convective systems over the tropical ocean. Part II: Heat and moisture budgets. *J. Atmos. Sci.*, **45**, 537–548, doi:10.1175/1520-0469(1988)045<0537:ACLCON>2.0.CO;2.

Fitzjarrald, D. R., and M. Garstang, 1981: Vertical structure of the tropical boundary layer. *Mon. Wea. Rev.*, **109**, 1512–1526, doi:10.1175/1520-0493(1981)109<1512:VSOTTB>2.0.CO;2.

Frank, W. M., 1978: The life cycles of GATE convective systems. *J. Atmos. Sci.*, **35**, 1256–1264, doi:10.1175/1520-0469(1978)035<1256:TLCOGC>2.0.CO;2.

Fueglistaler, S., A. E. Dessler, T. J. Dunkerton, I. Folkins, Q. Fu, and P. W. Mote, 2009: Tropical tropopause layer. *Rev. Geophys.*, **47**, 1004, doi:10.1029/2008RG000267.

Hartmann, D. L., H. H. Hendon, and R. A. Houze Jr., 1984: Some implications of the mesoscale circulations in tropical cloud clusters for large-scale dynamics and climate. *J. Atmos. Sci.*, **41**, 113–121, doi:10.1175/1520-0469(1984)041<0113:SIOTMC>2.0.CO;2.

Holloway, C. E., and J. D. Neelin, 2007: The convective cold top and quasi-equilibrium. *J. Atmos. Sci.*, **64**, 1467–1487, doi:10.1175/JAS3907.1.

Houze, R. A., Jr., 1977: Structure and dynamics of a tropical squall-line system. *Mon. Wea. Rev.*, **105**, 1540–1567, doi:10.1175/1520-0493(1977)105<1540:SADOAT>2.0.CO;2.

——, 1982: Cloud clusters and large-scale vertical motion in the tropics. *J. Meteor. Soc. Japan*, **60**, 396–410.

——, 1989: Observed structure of mesoscale convective systems and implications for large-scale heating. *Quart. J. Roy. Meteor. Soc.*, **115**, 425–461, doi:10.1002/qj.49711548702.

Johnson, R. H., 1984: Partitioning tropical heat and moisture budgets into cumulus and mesoscale components: Implications for cumulus parameterization. *Mon. Wea. Rev.*, **112**, 1590–1601, doi:10.1175/1520-0493(1984)112<1590:PTHAMB>2.0.CO;2.

——, and D. C. Kreite, 1982: Thermodynamic and circulation characteristics of winter monsoon tropical mesoscale convection. *Mon. Wea. Rev.*, **110**, 1898–1911, doi:10.1175/1520-0493(1982)110<1898:TACCOW>2.0.CO;2.

——, and G. S. Young, 1983: Heat and moisture budgets of tropical mesoscale anvil clouds. *J. Atmos. Sci.*, **40**, 2138–2147, doi:10.1175/1520-0469(1983)040<2138:HAMBOT>2.0.CO;2.

——, and X. Lin, 1997: Episodic trade wind regimes over the western Pacific warm pool. *J. Atmos. Sci.*, **54**, 2020–2034, doi:10.1175/1520-0469(1997)054<2020:ETWROT>2.0.CO;2.

——, and P. E. Ciesielski, 2000: Rainfall and radiative heating rate estimates from TOGA COARE atmospheric budgets. *J. Atmos. Sci.*, **57**, 1497–1514, doi:10.1175/1520-0469(2000)057<1497:RARHRF>2.0.CO;2.

——, and ——, 2002: Characteristics of the 1998 summer monsoon onset over the northern South China Sea. *J. Meteor. Soc. Japan*, **80**, 561–578, doi:10.2151/jmsj.80.561.

——, ——, and K. A. Hart, 1996: Tropical inversions near the 0°C level. *J. Atmos. Sci.*, **53**, 1838–1855, doi:10.1175/1520-0469(1996)053<1838:TINTL>2.0.CO;2.

Katsumata, M., P. E. Ciesielski, and R. H. Johnson, 2011: Evaluation of budget analysis during MISMO. *J. Appl. Meteor. Climatol.*, **50**, 241–254, doi:10.1175/2010JAMC2515.1.

Kiladis, G. N., M. C. Wheeler, P. T. Haertel, K. H. Straub, and P. E. Roundy, 2009: Convectively coupled equatorial waves. *Rev. Geophys.*, **47**, 2003, doi:10.1029/2008RG000266.

L'Ecuyer, T. S., and G. L. Stephens, 2003: The tropical atmosphere energy budget from the TRMM perspective. Part I: Algorithm and uncertainties. *J. Climate*, **16**, 1967–1985, doi:10.1175/1520-0442(2003)016<1967:TTOEBF>2.0.CO;2.

Leary, C. A., and R. A. Houze Jr., 1979: The structure and evolution of convection in a tropical cloud cluster. *J. Atmos. Sci.*, **36**, 437–457, doi:10.1175/1520-0469(1979)036<0437:TSAEOC>2.0.CO;2.

Lin, X., and R. H. Johnson, 1996: Kinematic and thermodynamic characteristics of the flow over the western Pacific warm pool during TOGA COARE. *J. Atmos. Sci.*, **53**, 695–715, doi:10.1175/1520-0469(1996)053<0695:KATCOT>2.0.CO;2.

Luo, H., and M. Yanai, 1984: The large-scale circulation and heat sources over the Tibetan Plateau and surrounding areas during the early summer of 1979. Part II: Heat and moisture budgets. *Mon. Wea. Rev.*, **112**, 966–989, doi:10.1175/1520-0493(1984)112<0966:TLSCAH>2.0.CO;2.

Mapes, B. E., and P. Zuidema, 1996: Radiative-dynamical consequences of dry tongues in the tropical troposphere. *J. Atmos. Sci.*, **53**, 620–638, doi:10.1175/1520-0469(1996)053<0620:RDCODT>2.0.CO;2.

——, P. E. Ciesieslki, and R. H. Johnson, 2003: Sampling errors in rawinsonde-array budgets. *J. Atmos. Sci.*, **60**, 2697–2714, doi:10.1175/1520-0469(2003)060<2697:SEIRB>2.0.CO;2.

Nicholls, M. E., R. A. Pielke, and W. R. Cotton, 1991: Thermally forced gravity waves in an atmosphere at rest. *J. Atmos. Sci.*, **48**, 1869–1884, doi:10.1175/1520-0469(1991)048<1869:TFGWIA>2.0.CO;2.

Nitta, T., 1978: A diagnostic study of the interaction of cumulus updrafts and downdrafts with large-scale motions in GATE. *J. Meteor. Soc. Japan*, **56**, 232–242.

——, and S. Esbensen, 1974: Heat and moisture budget analyses using BOMEX data. *Mon. Wea. Rev.*, **102**, 17–28, doi:10.1175/1520-0493(1974)102<0017:HAMBAU>2.0.CO;2.

Numaguti, A., R. Oki, K. Nakamura, K. Tsuboki, T. Asai, and Y.- M. Kodama, 1995: 4-5 day-period variations and low-level dry air observed in the equatorial western Pacific during the TOGA-COARE IOP. *J. Meteor. Soc. Japan*, **73**, 267–290.

Parsons, D., and Coauthors, 1994: The integrated sounding system: Description and preliminary observations from TOGA COARE. *Bull. Amer. Meteor. Soc.*, **75**, 553–567, doi:10.1175/1520-0477(1994)075<0553:TISSDA>2.0.CO;2.

Raymond, D. J., and H. Jiang, 1990: A theory for long-lived mesoscale convective systems. *J. Atmos. Sci.*, **47**, 3067–3077, doi:10.1175/1520-0469(1990)047<3067:ATFLLM>2.0.CO;2.

Redelsperger, J.-L., D. Parsons, and F. Guichard, 2002: Recovery processes and factors limiting cloud-top height following the arrival of a dry intrusion observed during TOGA COARE. *J. Atmos. Sci.*, **59**, 2438–2457, doi:10.1175/1520-0469(2002)059<2438:RPAFLC>2.0.CO;2.

Rickenbach, T. M., and S. A. Rutledge, 1998: Convection in TOGA COARE: Horizontal scale, morphology, and rainfall production. *J. Atmos. Sci.*, **55**, 2715–2729, doi:10.1175/1520-0469(1998)055<2715:CITCHS>2.0.CO;2.

Schumacher, C., and R. A. Houze Jr., 2003: Stratiform rain in the tropics as seen by the TRMM precipitation radar. *J. Climate*, **16**, 1739–1756, doi:10.1175/1520-0442(2003)016<1739:SRITTA>2.0.CO;2.

——, ——, and I. Kraucunas, 2004: The tropical dynamical response to latent heating estimates derived from the TRMM precipitation radar. *J. Atmos. Sci.*, **61**, 1341–1358, doi:10.1175/1520-0469(2004)061<1341:TTDRTL>2.0.CO;2.

——, M. H. Zhang, and P. E. Ciesielski, 2007: Heating structures of the TRMM field campaigns. *J. Atmos. Sci.*, **64**, 2593–2610, doi:10.1175/JAS3938.1.

Shie, C.-L., W.-K. Tao, J. Simpson, and C.-H. Sui, 2003: Quasi-equilibrium states in the tropics simulated by a cloud-resolving model. Part I: Specific features and budget analysis. *J. Climate*, **16**, 817–833, doi:10.1175/1520-0442(2003)016<0817:QESITT>2.0.CO;2.

Steiner, M., R. A. Houze, and S. E. Yuter, 1995: Climatological characterization of three-dimensional storm structure from operational radar and rain gauge data. *J. Appl. Meteor.*, **34**, 1978–2007, doi:10.1175/1520-0450(1995)034<1978:CCOTDS>2.0.CO;2.

Stull, R. B., 1985: A fair-weather cumulus cloud classification scheme for mixed-layer studies. *J. Climate Appl. Meteor.*, **24**, 49–56, doi:10.1175/1520-0450(1985)024<0049:AFWCCC>2.0.CO;2.

Webster, P. J., and R. Lukas, 1992: TOGA COARE: The Coupled Ocean–Atmosphere Response Experiment. *Bull. Amer. Meteor. Soc.*, **73**, 1377–1416, doi:10.1175/1520-0477(1992)073<1377:TCTCOR>2.0.CO;2.

Willis, P. T., and A. J. Heymsfield, 1989: Structure of the melting layer in mesoscale convective system stratiform precipitation. *J. Atmos. Sci.*, **46**, 2008–2025, doi:10.1175/1520-0469(1989)046<2008:SOTMLI>2.0.CO;2.

Yanai, M., 1961: A detailed analysis of typhoon formation. *J. Meteor. Soc. Japan*, **39**, 187–214.

——, S. Esbensen, and J.-H. Chu, 1973: Determination of bulk properties of tropical cloud clusters from large-scale heat and moisture budgets. *J. Atmos. Sci.*, **30**, 611–627, doi:10.1175/1520-0469(1973)030<0611:DOBPOT>2.0.CO;2.

Yoneyama, K., and T. Fujitani, 1995: The behavior of dry westerly air associated with convection observed during TOGA-COARE R/V *Natsushima* cruise. *J. Meteor. Soc. Japan*, **73**, 291–304.

Zipser, E. J., 1969: The role of organized unsaturated convective downdrafts in the structure and rapid decay of an equatorial disturbance. *J. Appl. Meteor.*, **8**, 799–814, doi:10.1175/1520-0450(1969)008<0799:TROOUC>2.0.CO;2.

——, 1977: Mesoscale and convective-scale downdrafts as distinct components of squall-line circulation. *Mon. Wea. Rev.*, **105**, 1568–1589, doi:10.1175/1520-0493(1977)105<1568:MACDAD>2.0.CO;2.